



Fabric steering technology for variable stiffness panels: Manufacture and mechanical testing

Zhaofei Xiao^{a,b,*}, Philip Harrison^b

^a ASTUTE2020, College of Engineering, Swansea University, Swansea, SA1 8EN, UK

^b James Watt School of Engineering, University of Glasgow, Glasgow, G12 8QQ, UK

ARTICLE INFO

Keywords:

Variable stiffness laminates
Buckling
Failure
Fabric steering

ABSTRACT

A novel low-cost manufacturing process is introduced, referred to as 'Fabric Steering'. By manipulating biaxial fabrics, curvilinear fibre paths can be created to manufacture variable stiffness panels, similar to those produced using Automated Fibre Placement [1]. With low equipment costs and the capability to steer multiple-layers of fabrics simultaneously, this technique potentially offers faster production rates and lower manufacturing costs compared to Automated Fibre Placement. A computer aided engineering tool, SteerFab [2,3], is used to guide the design and manufacture process by predicting: (a) the optimum 2D fibre paths, (b) the subsequent mechanical behaviour of the resulting variable stiffness panel (including improvements in buckling resistance and strength) and (c) step-by-step manufacturing instructions. Compared to conventional quasi-isotropic straight-fibre laminates, experimental buckling tests show slightly heavier (by 4.6%) steered-fibre laminates achieve improvements of ~9% and ~17% in buckling resistance load and failure load, findings that fit well with numerical predictions.

1. Introduction

Despite relatively high material and manufacture costs, carbon fibre composites are widely used in the aerospace industry due to their exceptional specific mechanical properties. The pressure to reduce manufacture costs and improve both performance and quality has led to the development of automated processes. Automated Fibre Placement (AFP) is a robotic layup technology that can deposit single or multiple prepreg fibre tows with a width range of between 3 and 13 mm [4]. The targeted placement of individual tows by AFP has offered new design opportunities. For example, researchers have explored the possibility of using AFP to manufacture parts containing curvilinear rather than straight fibre paths, manufacturing so called 'Variable Stiffness Panels' (VSP) [1,5–7]. According to Refs. [1,5,6,8,9], AFP-manufactured VSP can achieve 10% improvements in buckling load and 25% increases in failure load when compared to straight-fibre laminates of the same weight. The potential application of VSP in aircraft structures, such as fuselage T-shaped stiffened skin panels and wings, has already been considered [10–12]. However, manufacture of VSP via AFP processing is not without its problems. During production, the high in-plane bending and shearing stiffness of prepreg fibre tows tend to cause three typical types of defect: tow overlaps, tow gaps and tow-wrinkles [7,13–15]. To

overcome these issues, Continuous Tow Shearing [14–16], a new variant of AFP technology has been developed. Continuous Tow Shearing manipulates prepreg tapes or dry fibre tows to create defect-free curvilinear fibre paths [14–16]. While these fibre placement technologies demonstrate an extremely promising capability to manufacture highly optimised steered-fibre structures, they are limited to deposit tapes or tows with finite widths that are considerably smaller than the size of the part to be produced, and high capital costs for the sophisticated robots can lead to high part costs. The motivation behind the current work is to demonstrate a route to manufacture steered-fibre structures via deformation of fabric and composite prepreg sheets, rather than via AFP-style additive manufacture. The approach eliminates the high capital costs associated with AFP but does currently require significant labour. The latter could be reduced with technical innovation but for now the main advantage of the method is that it can be performed without access to expensive equipment and can be used with a wide variety of fabrics.

Traditional composite forming is a popular mainstream manufacture process due to its high production rate. The process allows large multi-layer sheets to be formed quickly in a single step into complex shapes [17]. The importance of this process has led to a significant body of research dedicated to understand engineering fabric and advanced composite prepreg forming mechanics, including predictions of fibre

* Corresponding author. ASTUTE2020, College of Engineering, Swansea University, Swansea, SA1 8EN, UK.

E-mail address: zhaofei.xiao@swansea.ac.uk (Z. Xiao).

<https://doi.org/10.1016/j.compositesb.2021.109105>

Received 22 April 2020; Received in revised form 27 January 2021; Accepted 24 June 2021

Available online 30 June 2021

1359-8368/© 2021 The Authors. Published by Elsevier Ltd. This is an open access article under the CC BY license (<http://creativecommons.org/licenses/by/4.0/>).

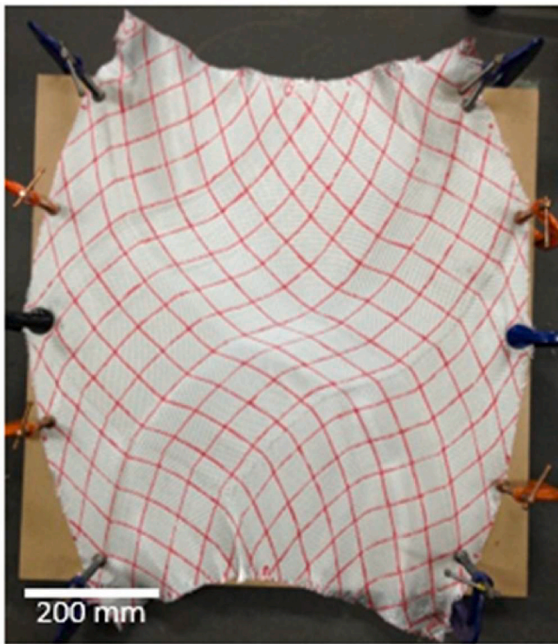


Fig. 1. The initial manually steered fabric showing curvilinear fibre path.

orientations and sheet wrinkling [17–27]. Forming models range from simple kinematic pin-jointed net approaches [18] to comprehensive constitutive models implemented in finite element codes that include the fibre tensile stiffness, fabric shear stiffness, in-plane and out-of-plane bending stiffness, torsional stiffness, through thickness stiffness and both inter-ply and tool-ply friction [19–27]. Composites forming is inherently recognised as a three-dimensional (3D) manufacturing process, however, this investigation explores the use of two-dimensional (2D) in-plane forming of regular engineering fabrics/prepregs to create desirable steered fibre patterns to tailor stiffness of composite panels. A Matlab®-based numerical design and analysis tool, SteerFab [2,3], has been specifically developed to support this 2D forming technique, both in determining how to steer the fabric and in predicting the final ideal steered fibre pattern and laminate layup for optimum mechanical properties. The steered-fibre patterns generated from SteerFab are based on trellis shear kinematics and the mechanism of SteerFab is described in detail in Ref. [3]. Comprehensive finite-element simulations [28] may be used to model the fabric steering process in future.

The aim of this investigation is to develop a novel 2D fabric forming process which is able to rapidly manufacture steered-fibre laminates

with improved mechanical properties. Hence, this paper focuses first on the development of the 2D fabric steering process, including the introduction of the basic principles of 2D fabric steering and a series of tests to address questions about the repeatability and the influence of processing factors. In addition, the SteerFab is used to: (a) guide the manufacture process and (b) predict the laminate's final mechanical properties. Several simplifying assumptions are made in the modelling process (discussed in the coming sections) and so very accurate predictions are not expected, rather the goal is to show how SteerFab can be used to predict the general trends shown in the experimental data, demonstrating that the 2D fabric steering technology is supported and corroborated by numerical analysis.

2. Two-dimensional fabric steering

Even though the purpose of the uniaxial bias extension test [29–31] is not aimed at fibre steering, the test is nevertheless a simple and familiar example of 2-D fabric forming. In the early stages of the uniaxial bias extension test, the sample remains planar while the initially straight fibre directions across the specimen become curvilinear as the tows run through one region of the sample to the next. Fibre steering is induced simply by constraining and displacing part of the test specimen's perimeter, the fibre directions across the specimen are reasonably predictable as the fabric deforms, more or less, according to pin-jointed net kinematics [18]. In a similar way, steered fibre patterns can be induced in engineering fabrics by hand, simply by manipulating the perimeter of a sheet. An example is shown in Fig. 1 which shows a sheet of woven glass fabric manipulated and then fixed in position using G-clamps. The steered pattern can also be fixed in position, without the use of G-clamps, via the application of adhesive binder sprayed onto the fabric. Similar steered patterns can be generated using SteerFab, see Fig. 2, which shows the fabric shape before and after deformation. Theoretically, the technique of manipulating the perimeter of the specimen can be used to create a more complex laterally repeating steered-fibre pattern, see for example, Fig. 3A. However, if even more challenging steered fibre patterns, tessellating in both the lateral and vertical directions are to be manufactured (see Fig. 3B), simple manipulation of the perimeter of the specimen does not provide sufficient control. To do this, another technique, multi-point manipulation, has been developed. The concept behind this technique involves displacing internal points to target end-point positions, which can be predicted via pin-jointed net kinematics using SteerFab. The latter lets users clearly see how any given point within the fabric should move and serves as a guide to the fibre steering process. The user can select an arbitrary number of nodes, the code then shows initial and final positions of the nodes and red lines show their motion paths. As an example, Fig. 4 shows the motion path of

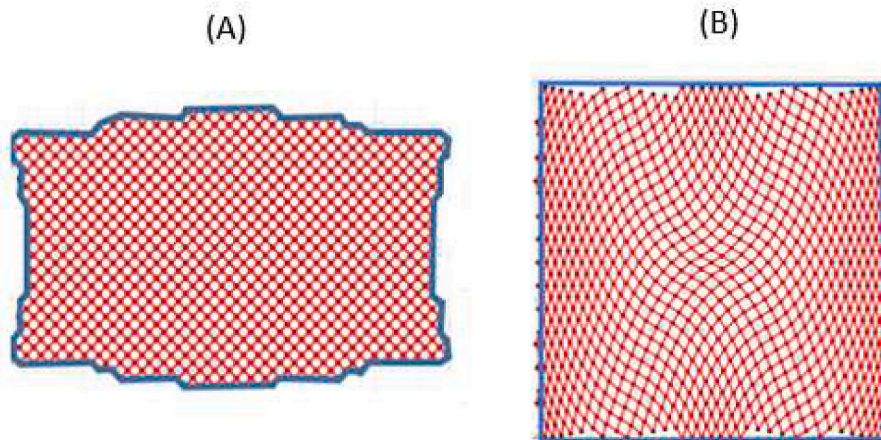


Fig. 2. (A) Initial unsheared shape and (B) a steered pattern generated by the SteerFab code (similar to Fig. 1).

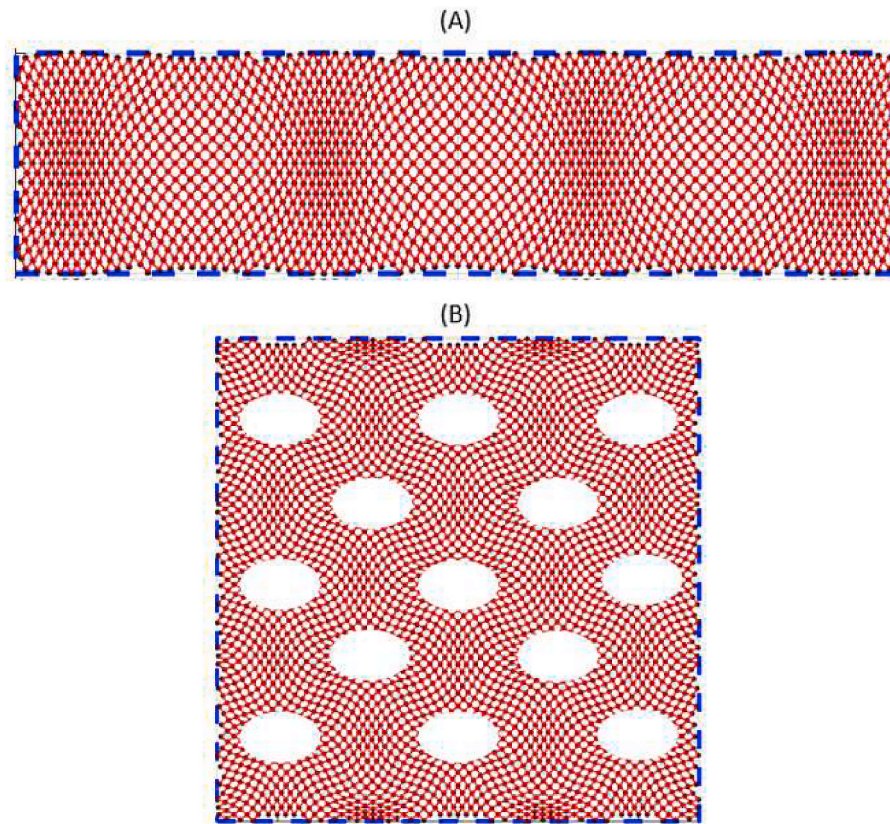


Fig. 3. Steered-fibre patterns: (A) laterally repeating and (B) tessellating in both the lateral and vertical directions, with elliptical holes.

pre-selected nodes. The method currently uses nylon fishing lines to pierce selected points of the undeformed fabric at the manipulation control points. To reduce possible fabric damage caused by concentrated loading by the threaded line, buttons are used to reduce stress concentrations. Fig. 5 schematically shows the detailed threaded structure. The nylon line is also threaded through holes drilled in a Perspex sheet; the position of the holes in the Perspex sheet correspond with the final position of nodes in the target steered fibre pattern. Hence, by pulling the threads into place, desirable steered fabric patterns can be manufactured.

2.1. Controlling the fabric steering process

An important goal of the multi-point manipulation manufacture process is to achieve the steered fibre pattern as closely as possible, without defects, and ideally without using any manual hand manipulation. Three important questions regarding successful fabric steering arise, namely: (1) How to best select control points? (2) What is the repeatability of the steering process? and (3) Does the manipulation order affect the final steered pattern and the generation of forming defects (e.g. out-of-plane wrinkling)?

To answer these questions, two experiments were conducted. The first to examine process repeatability and the second to understand the effect of manipulation order. In both experiments, the steered pattern predicted by the kinematic model was divided into a 5×5 grid, with a control point at each corner. Nodes were numbered, as shown in Fig. 4A and B. The SteerFab code predicted the initial and final positions of the control points (Fig. 4C). The initial positions were marked on the fabrics for threading of the line and buttons, and holes (diameter of 2 mm) were drilled in a Perspex sheet based at the final positions, as discussed in Section 2.1. A plain-woven glass fibre fabric (ECK 10–300 gsm from Allscot) was used to conduct these two experiments. Each sample consisted of two aligned sheets of fabric, and a thin layer of adhesive (3 M

Spray Mount) was applied between the two sheets to improve integrity and cohesion, reducing damage caused by the nylon line when the latter was placed under tension.

2.1.1. Process repeatability

In the repeatability experiment, a manipulation order (Order 1 in Table 1) was selected. This test was repeated three times. Photographs were taken after each manipulation step to compare the shape of the deformed fabric at the same stage in each repeat experiment. Fig. 6A–6C show the final steered patterns of the three samples using the identical manipulation order (Order 1 in Table 1) and Fig. 6D demonstrates the comparison of fibre paths from those three steered samples (Fig. 6A–C). The patterns and shapes look similar and the fibre paths are also matched to each other. Furthermore, the locations of wrinkles created by the manipulation are the same in each repeat (see Appendix A), indicating good process repeatability.

2.1.2. Influence of manipulation order

To investigate the effect of manipulation order on the final pattern, three different manipulation orders were studied. The details of each order are also listed in Table 1. Fig. 7A–C show the steered patterns created by the three manipulation orders, and Fig. 7D demonstrates the comparison of their fibre paths. There is no major difference between the patterns created by Order 1 and Order 2 (Fig. 7A, B). However, when comparing the patterns created by a completely reverse manipulation order (Fig. 7B, C), one distinct difference is the presence of wrinkles in the regions highlighted by the blue rectangle and the fibre path of Order 3 (dot line in Fig. 7D) shows the largest discrepancy to the fibre paths of Order 1 and Order 2. This is caused by differences in the development of wrinkles during the forming process. The figures provided in Appendix A and B, show that after the 1st manipulation, both Order 1 and Order 2 have a large wrinkle along the vertical centreline, as the displacements of the manipulated points at the first step creates in-plane compression

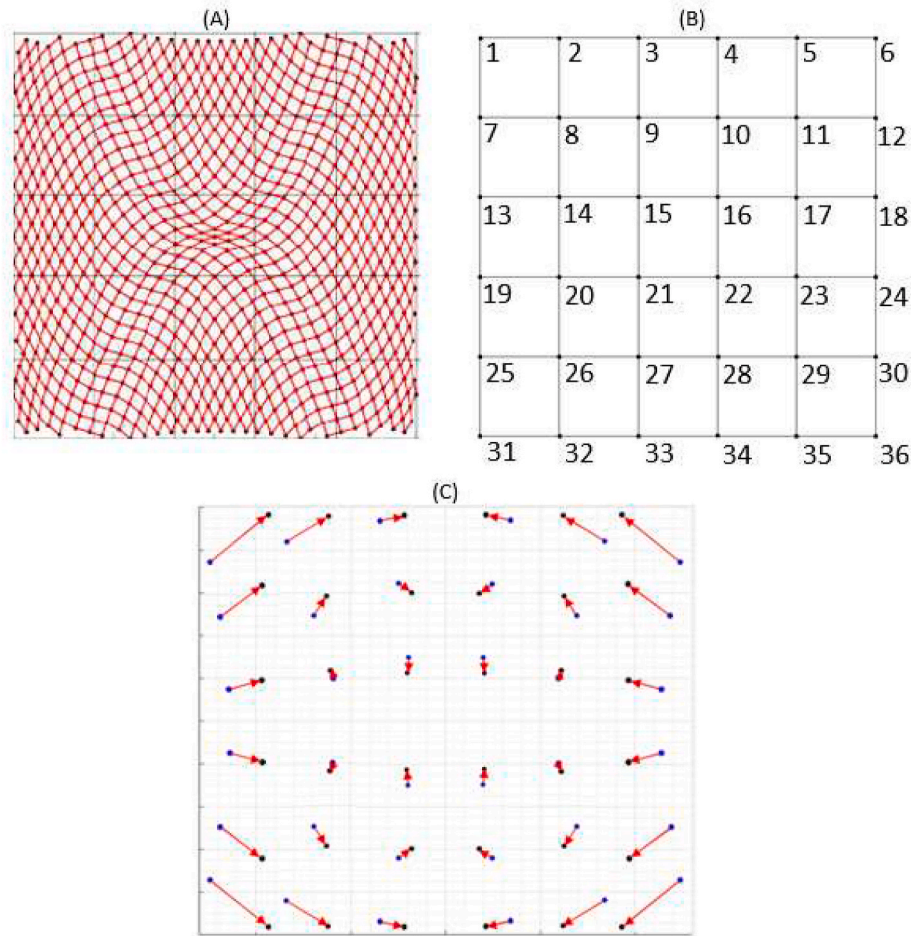


Fig. 4. (A) A steered fibre pattern, (B) control points selection and associated numbering and (C) the initial (blue) and final positions (black) of the selected control points. (For interpretation of the references to colour in this figure legend, the reader is referred to the Web version of this article.)

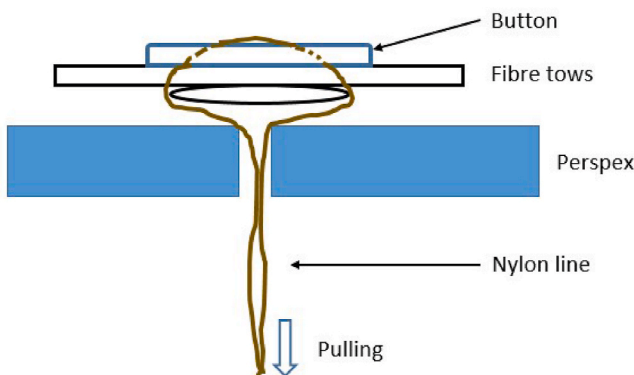


Fig. 5. The schematics of the threading set-up of the multi-point manipulation approach.

towards the centreline and applies compressive loads to the fabric accordingly. The very low out-of-plane bending stiffness makes fabrics likely to buckle out-of-plane, because compared to the compression strain energy, the bending strain energy for an out-of-plane displacement is much smaller [32]. Because the kinematic model contains only very basic assumptions such as fibre inextensibility and zero shear stiffness, it is unable to predict more complex behaviour such as buckling and is therefore only able to provide a rough approximation of the actual fabric kinematics. In addition, because the displacements of the points highlighted by the blue rectangle cannot provide sufficient tension to

eliminate wrinkles. Once the latter have formed, they persist to the final state. In contrast, the manipulations in Order 3 did not generate wrinkles along the vertical centreline. Wrinkles highlighted by the red rectangles occur in all specimens, irrespective of the manipulation order. This is also because the displacements of the four points within this region are all directed towards the centre of the steered fibre pattern, so the fabric is under compression (though an alternative choice of control points could potentially solve this issue).

Based on these results, there appear to be two techniques to reduce wrinkles during fabric steering:

- Avoid generation of large-scale wrinkles early in the forming process by manipulating control points having the smallest displacements first. This serves to locally constrain the out-of-plane displacement of the fabric to increase out-of-plane bending strain energy, so that the later manipulations are less likely to introduce wrinkles.
- Where possible, select control points which apply tension to shear the fabric during their displacements, in order to avoid applying compressive load.

Additionally, in Ref. [33], the authors demonstrated how Perspex sheet could be used to mitigate the formation of large wrinkles in the uniaxial bias extension test. The same concept can be applied in this fabric steering process. During the multi-point manipulation, the fabric is placed between the workbench surface and a Perspex sheet. Weights are placed on the Perspex sheet to add extra compaction pressure in the normal direction to constrain out-of-plane displacement across the whole sheet of fabric. A schematic of the set-up is shown in Fig. 8.

Table 1

The investigated manipulation orders and the corresponding schematics.

Order No.	Order description	Schematics (Numbers indicate sequence)
1	Outside corners → Centre → Towards outside	
2	Outside perimeter → Towards centre	
3	Centre → Perimeter (Completely reverse order of Order 2)	

2.2. Thickness change after fabric steering

Through using the multi-point manipulation approach, the manipulated fabric is sheared at different levels across the whole fabric according to the displacements of the selected control points. Hence, the thickness of the fabric will change accordingly with the shearing levels.

In a previous study about CTS [34], the material is treated as incompressible with a constant fibre volume fraction, which is a reasonable approximation for prepreg materials. Hence, the local thickness of the steered sheet, T , is calculated as:

$$T = T_0 / \cos\theta \quad (1)$$

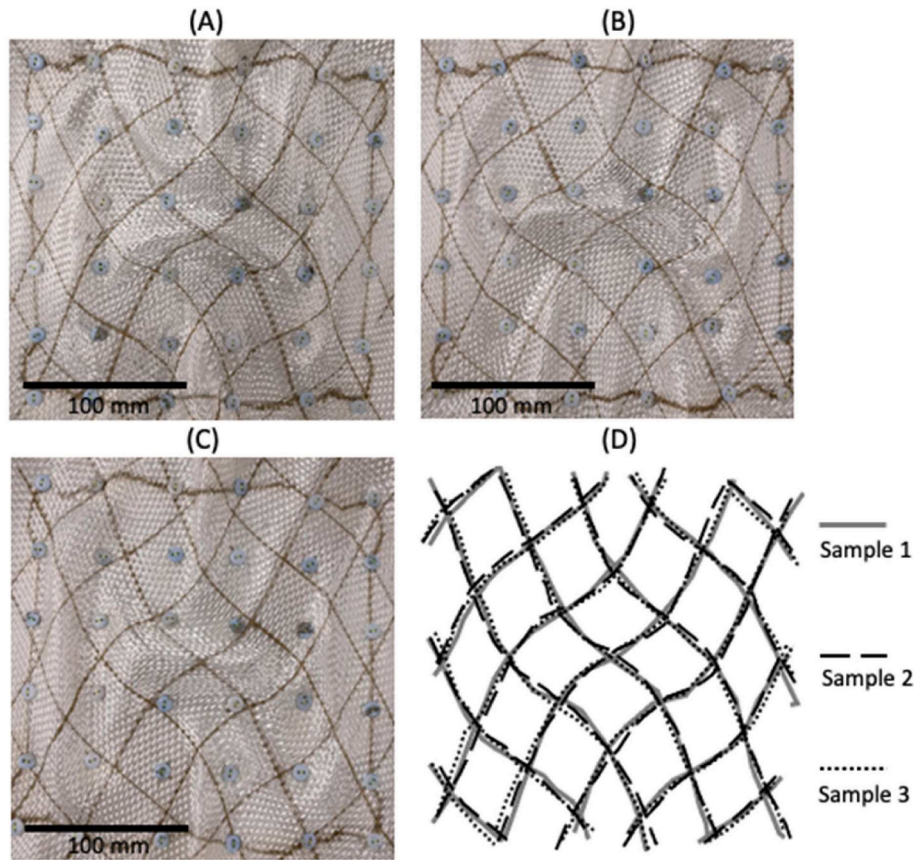


Fig. 6. Final steered patterns created by using Order 1: (A) sample 1; (B) sample 2; (C) sample 3, and (D) comparison of fibre paths from three samples.

where T_0 is the thickness of the undeformed sheet and θ is the shear angle.

In this paper, the thickness versus shear angle behaviour of the glass-fibre fabric is measured. To do this the thicknesses of moulded laminates containing 8 sheets of fabrics sheared to various shear angles (0° ; 10° ; 20° ; 30° ; 40° ; 50°) were measured to determine a realistic thickness versus shear angle behaviour. The data is shown in Fig. 9 and the fitted equation is given by Equation (2).

$$T = 6 \times 10^{-6} \times \theta^3 - 3 \times 10^{-4} \times \theta^2 + 7.3 \times 10^{-3} \times \theta + T_0 \quad (2)$$

where θ is measured in degrees. From Fig. 9, it can be seen that there is a discrepancy between the two thickness models, because the dry plain woven glass fabric (from Allscott) used in this investigation is more compressible than the cross-ply prepreg materials used in Ref. [34]. Hence, when the fabric is sheared, the fibre tows are more compacted, leading to higher fibre volume fraction, so thickness will not increase as much as the thickness model of the incompressible prepreg material.

To manufacture the pre-sheared laminates, 8 undeformed sheets of the Allscott plain woven glass fabric, measuring $80 \text{ mm} \times 80 \text{ mm}$, were aligned and stacked together. 3 M adhesive spray was applied between each layer of fabric. The 8-sheet stack of fabric was then sheared to a given shear angle by pulling diagonally opposing corners of the fabric stack. After deformation, weights were placed on the two corners of the fabric stack to maintain the shape of the sheared fabric. An image of the laminate was taken from the top view and ImageJ [35] was used to measure the shear angles at five evenly distributed points along the longer diagonal length of the fabric stack. The average angle was calculated to represent the shear angle of this specimen. Once the adhesive was cured (to retain the specimen shape), the laminate was moulded by vacuum infusion. After curing the thickness at the five points were measured to find the average thickness of the composite

laminate. The standard deviation (SD) of the measured shear angle and thickness are represented by the horizontal and vertical error bars (± 1 SD) shown in Fig. 9.

3. Buckling tests

The multi-point manipulation approach to fabric steering was used to manufacture steered-fibre ply (SFP)/straight-fibre ply hybrid $[(\pm \text{SFP})_2 / (90/0)_2]_s$ laminates that have been numerically predicted in Refs. [2,3] to have better buckling resistance than conventional QI laminates, i.e. $[(\pm 45)_2 / (90/0)_2]_s$. Buckling resistance can be experimentally measured in a buckling test. It should note that the hybrid laminate is slightly heavier (by $\sim 4.6\%$ as shown in Table 2) than the straight-fibre laminates, because of the fabric area change after steering. The same fabric as that used in the process investigation (see Section 2) was used to manufacture the laminates. After the steered fabric sheets were manufactured via the multi-point manipulation approach, facilitated by predictions of the SteerFab code, both steered and straight fibre fabric sheets were laid up in the optimal stacking sequence for subsequent vacuum infusion moulding using IN2 Epoxy (from EasyComposites). Fig. 10 demonstrates the match between the steered fabric, the kinematic model prediction and the final composite laminate using the optimal steered pattern found in Refs. [2,3]. The orientation of the fibres is $\approx 45^\circ$ at the centre of steered pattern and gradually reaches $\approx 60^\circ$ at the intersection of the vertical edge and the horizontal centreline, because the shear angle, θ_i , at the intersection reaches $\approx 30^\circ$ as shown in Fig. 10D. Note that the shear angle along the vertical edge is not necessarily the same as the θ_i , due to the mesh generation algorithm used by SteerFab [3].

3.1. Buckling test set-up

The resulting panels were sprayed with a speckle-pattern to permit

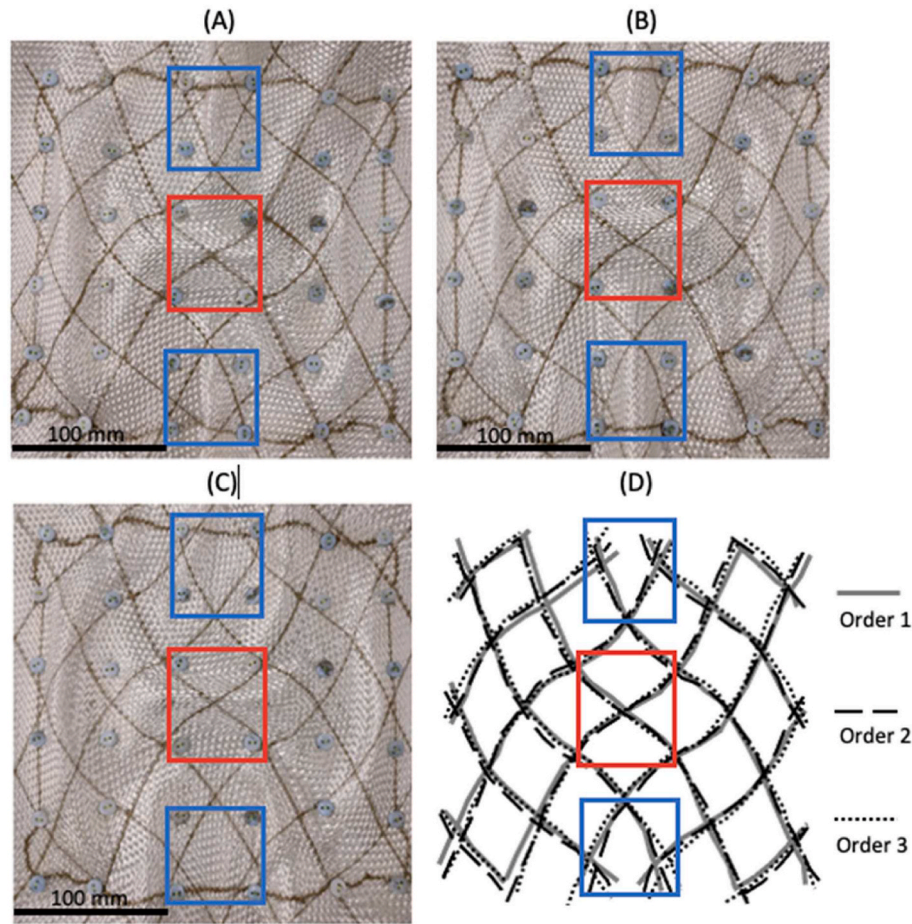


Fig. 7. Final steered patterns created by using (A) Order 1; (B) Order 2; and (C) Order 3, and (D) comparison of fibre paths using three orders.



Fig. 8. Schematic of surface constrain set-up to eliminate wrinkles.

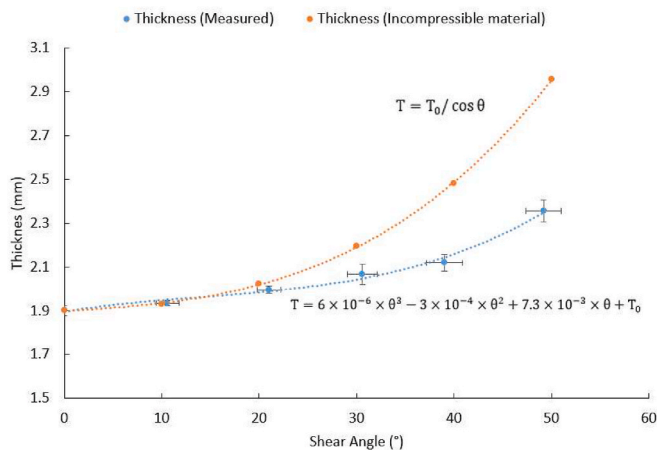


Fig. 9. Measured thickness of 8-sheet plain woven glass fabrics at different shear angles and the thickness calculated by assuming the fabric is an incompressible material. Error bars are standard deviations (± 1 SD) of the measured shear angles and thicknesses.

Table 2

Mass measurement results of the specimens for buckling test.

Mass (g)	QI Laminates $[(\pm 45)_2/(90/0)_2]_s$	Hybrid Laminates $[(\pm SFP)_2/(90/0)_2]_s$
1	461.0	475.6
2	455.4	478.5
3	458.8	484.4
Average	458.4	479.5 (+4.6%)

stereoscopic Digital Image Correlation (DIC) using a VIC 3D DIC system (Correlated Solutions, Inc.), in order to track displacements and from there to calculate surface strains during buckling tests. The two cameras were placed at a distance of 300 mm away from the specimen and the VIC-3D 2010 software was used to analyse the resulting images. A subset size of 30×30 pixels was used to analyse the data. Regarding the speckle-pattern, one side of each specimen was sprayed with white paint (Plasti-kote 3100SE) over its entire surface. A black speckle pattern (Black spray paint from Canbrush) was then applied by obliquely spraying the specimen allowing relatively large paint droplets to uniformly and randomly fall onto the specimen surface. The panels were then trimmed to a size of 310×460 mm. The testing area measured 300×400 mm, after each specimen was mounted in a buckling testing rig, designed based on the experiments reported in Ref. [8], and manufactured specifically for this investigation. The diameter of the circular cut-out positioned at the centre of each panel was 90 mm. In the test, the testing rig was clamped in a universal mechanical test machine (ZwickRoell Ltd Z250), and the upper cross-head beam was moved down at a rate of 1 mm/min. The test set-up is shown in Fig. 11A. The bottom edge of the specimen was fully fixed by clamps, and the top edge was

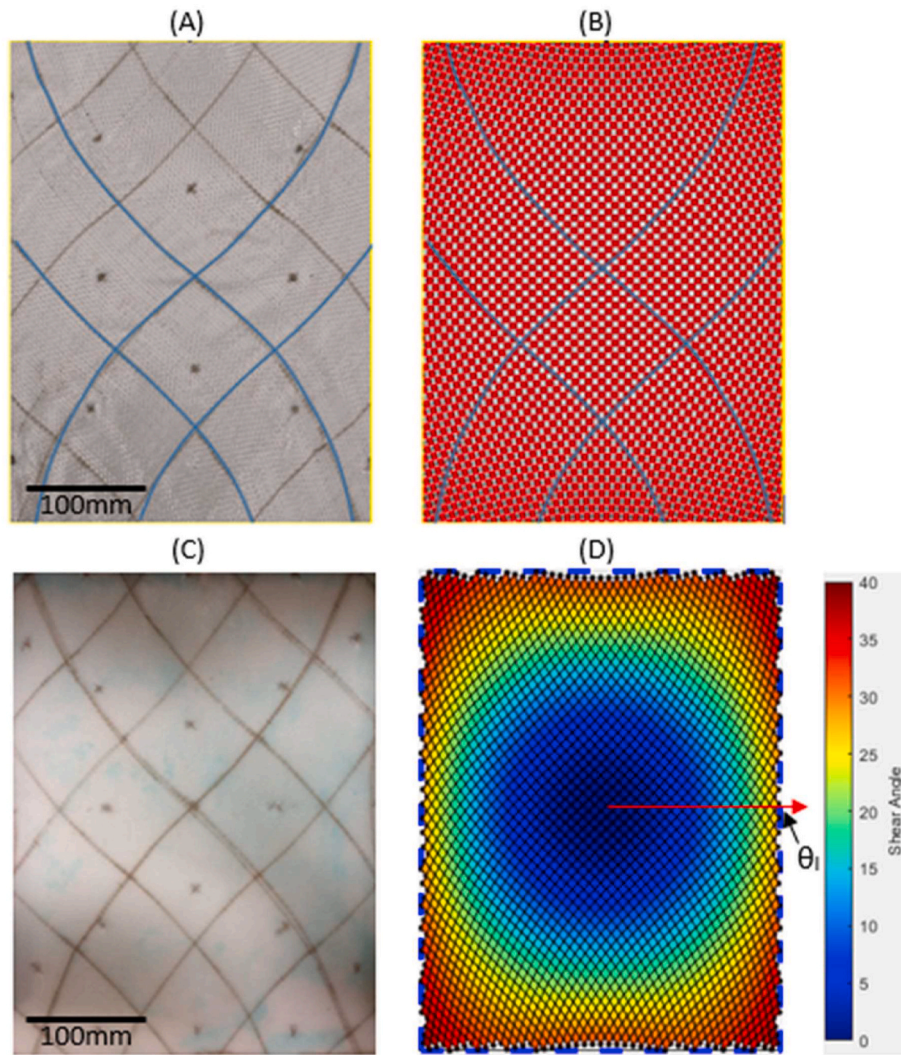


Fig. 10. Comparison among the 300 mm \times 400 mm (A) manufactured steered fabric; (B) steered pattern created by SteerFab; (C) moulded steered fabric laminates; and (D) the shear angle map of the steered pattern shown in (B).

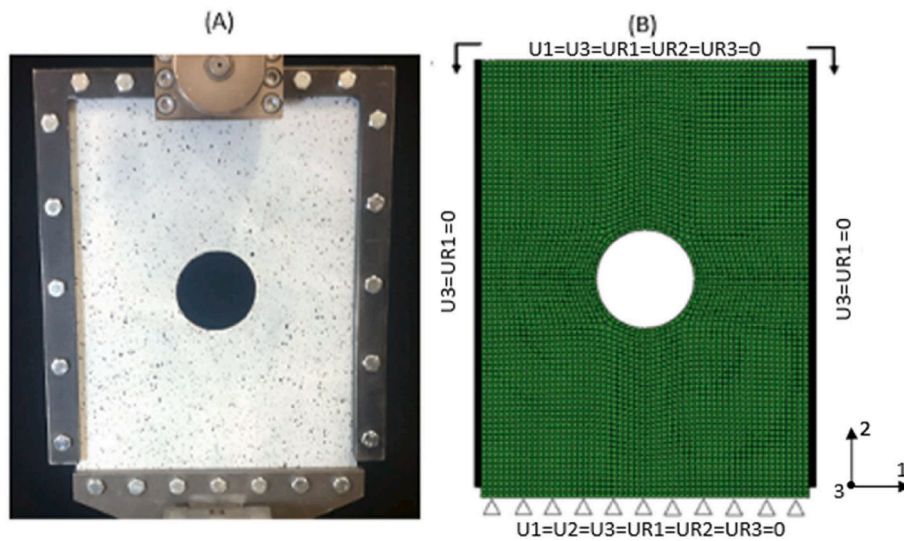


Fig. 11. (A) Buckling test set-up including test specimen with applied speckle pattern for DIC testing and (B) the schematic of the corresponding boundary conditions in simulation. The specimen size is 300 mm \times 400 mm within the testing frame and hole diameter is 90 mm.

Table 3
Mechanical properties of the glass composites used in the simulation.

Materials	E glass fibre-epoxy system
Data source	[41]
Material properties ^a	E ₁₁ : 41.0 GPa E ₂₂ : 10.4 GPa ν_{12} : 0.28 G ₁₂ : 4.7 GPa X _t : 1140 MPa X _c : 620 MPa Y _t : 39 MPa Y _c : 128 MPa S: 89 MPa
Ply thickness ^b	0.1188 mm

^a Note that this data is material properties of glass-fibre UD ply. E is Young's modulus; G is shear modulus; ν is Poisson's ratio; X_t and X_c are the tensile and compression strengths at fibre longitudinal direction; Y_t and Y_c are the tensile and compression strengths at fibre transverse direction; S is shear strength.

^b The ply thickness is one sixteenth of the measured thickness (1.90 mm) of a laminate containing 8 sheets of fabrics which is estimated as 16 plies in the simulation.

clamped to only allow the displacement at the vertical direction. The out-of-plane displacement and rotation about the horizontal direction on the two side edges are constrained by the frame of the testing rig. For each type of laminate, three specimens were tested.

3.2. Finite element model

A finite-element model (Fig. 11B) with size 300 × 400 mm was created in Abaqus 2017 to conduct post-buckling analysis, for comparison with the experiments. The size of the S4R elements used in the model is 5 × 5 mm. A mesh sensitivity study using a finer mesh comprised of 19,200 elements (each measuring about 2.5 × 2.5 mm) revealed a change of just 0.6% in the predicted buckling load, suggesting the 4800-element mesh is a reasonable compromise between speed and accuracy. Fig. 11B also shows a schematic of the boundary conditions. An 'encastre' condition (U1 = U2 = U3 = UR1 = UR2 = UR3 = 0) is applied on the bottom edge, whilst for the top edge only displacement at the vertical direction is allowed (U1 = U3 = UR1 = UR2 = UR3 = 0) and a load of -1N is applied on each element along the length of the top edge. Out-of-plane displacement and rotation about the horizontal direction on the two side edges (indicated by thick black lines in Fig. 11B), are constrained (U3=UR1 = 0). The linear 'Perturbation - Buckle' in Abaqus followed by the 'General - Riks' method [36] was used for the post-buckling simulation. Stiffness predictions use assumptions of Classical Laminate Theory [37]. Strength predictions are made using

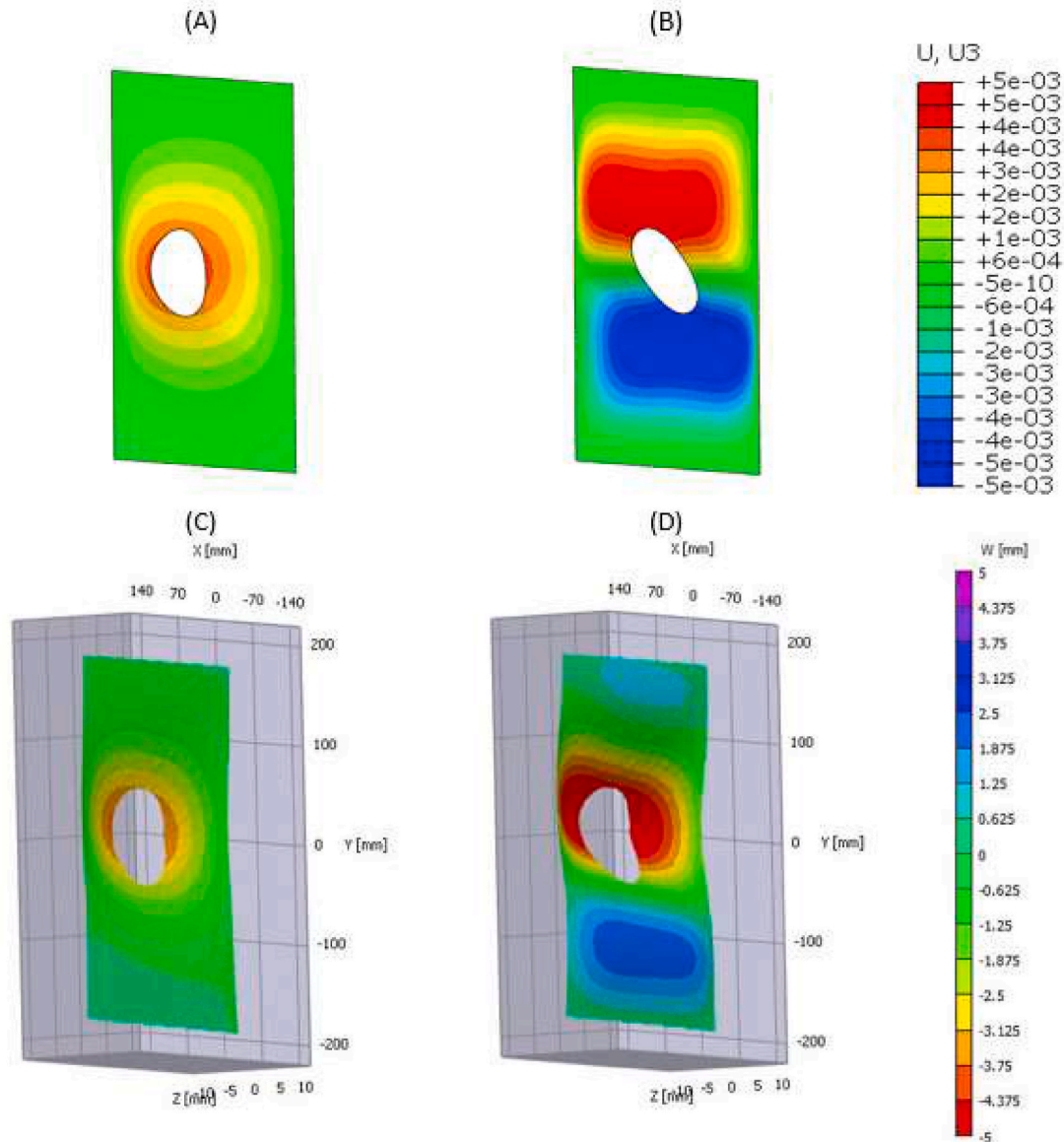


Fig. 12. Typical 1st and 2nd buckled geometries of the steered/straight hybrid laminate specimens from (A)–(B) post-buckling simulation in Abaqus and (C)–(D) 3D DIC images.

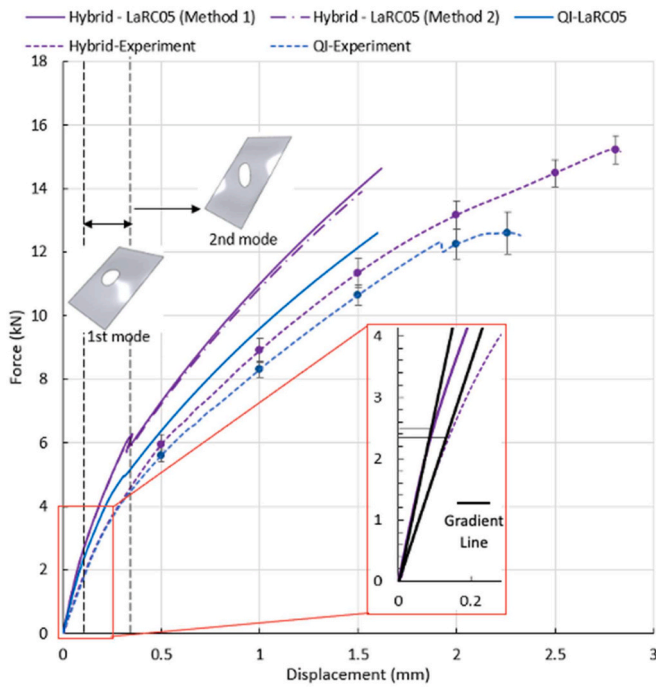


Fig. 13. Force-Displacement curves from post-buckling simulations (LaRC05 damage model; Thickness assumption Method 1 and Method 2) and experiments of the QI and steered/straight hybrid laminates. Error bars are standard deviations (± 1 SD) of measured forces at different displacement levels. The image in the red region shows the initial parts of the curves of the hybrid laminate from simulation and experiment as examples in order to demonstrate the determination of buckling loads from gradient change. (For interpretation of the references to colour in this figure legend, the reader is referred to the Web version of this article.)

two different damage models already implemented in Abaqus, namely the Hashin [38] and LaRC05 [39,40] models. Individual UD glass-fibre ply properties, obtained from Ref. [41], are listed in Table 3. Note that, because the FE model uses Classical Laminate Theory to model the composite properties, each sheet of fabric is approximated as two plies. Although this estimation ignores the fibre tow crimp in the woven fabric, simulation results still reflect the effect of continuously-changing the fibre orientation on buckling resistance. Both the steered/straight hybrid laminate and the QI straight-fibre laminate contained 8 sheets of fabric, so each laminate contained 16 plies in the simulation.

The tow angle and thickness of the generated steered patterns are mapped via the SteerFab code to the finite-element model for buckling analysis [2,3]. Each steered pattern provides orientation information for two distinct steered fibre plies, named here as (\pm SFP). As mentioned at the beginning of Section 2.2, the fabric area changes after steering, so the sheet thickness and the areal density associated with the fibre volume fraction will also change. The continuously changing fibre volume fraction across the whole FE mesh means that each element within the mesh should ideally have its own material properties. However, this

approach would lead to high computational cost. Hence, in the current investigation, two thickness approximation methods, which are introduced in Section 2.2, have been used to reasonably simplify the simulations.

The first thickness assumption used in the structural simulations, Method 1, over-estimates the thickness versus shear angle behaviour by ignoring fabric compaction, while the second assumption, Method 2, uses the measured thickness versus shear angle behaviour but ignores changes in the fibre volume fraction. According to Ref. [42], the critical buckling load of a plate increases with the cube of its thickness, whilst the load increases linearly with the Young's modulus, which also has a linear relationship with fibre volume fraction. Hence, the simulations provide upper and lower predictions of the structural properties of the steered/straight hybrid laminate (ignoring reductions in stiffness related to the crimping of the tows). Using Method 1, the average thickness of the 16-ply hybrid laminate ($[(\pm$ SFP) $_{2/(90/0)}]_{2s}$) is 1.983 mm, which is $\sim 4.3\%$ thicker (heavier) than the 16-ply straight-fibre laminate (measured thickness of 1.90 mm). Using Method 2 the hybrid laminate is 1.963 mm thick on average, making the laminate $\sim 3.3\%$ heavier than the straight-fibre laminate.

3.3. Comparisons of simulation and experiment results

Fig. 12 demonstrates the typical forms of the 1st and 2nd mode buckles across the steered/straight glass fibre hybrid laminates both, (i) predicted by post-buckling simulations (Fig. 12A, B) (ii) recorded by the 3D DIC equipment (Fig. 12C, D). Corresponding force versus displacement predictions and measurements are shown in Fig. 13. The displacement of the experiment is the DIC measurement for the end shortening of the specimen test area. The change in gradient and the associated transition from a linear to a non-linear force versus displacement curve indicates the onset of the 1st buckling mode (as demonstrated by the enlarged image in the red region of Fig. 13), while the change in non-linearity indicates the onset of the 2nd mode. Note that the buckling load determined by the gradient change for each force-displacement curve from either Riks analysis or experiment was the average value of three measurements and the straight gradient line was re-drawn in each measurement. The error bars on the experimental data points represent ± 1 standard deviation from the average force values at different displacement levels. Values for the 1st buckling mode and failure load of both straight fibre and steered/straight fibre laminates are listed in Table 4.

Compared with the manufactured straight fibre QI laminates, the buckling load (1st mode) of the manufactured steered/straight hybrid laminate is improved by 9.1%, which falls into the predicted improvement levels suggested by numerical simulations (9.6% using the thickness assumption of Method 1 and 8.3% using Method 2). In addition, the experimental data suggests the improvement in failure load of the manufactured hybrid laminates over the manufactured straight fibre laminates is even more significant (16.8%) than the increase in the buckling load. Predictions using Method 1 for the thickness versus shear angle behaviour, of both the Hashin [38] and LaRC05 [39,40] damage models also reflect similar levels of improvement (17.4% and 16.1% respectively) in the failure load. The LaRC05 model provides a closer

Table 4
The experimental and predicted buckling resistance properties of two plain woven glass fibre laminates.

Glass Fibre		Numerical simulation				Experiment	
		Buckling load (kN)		Failure load (kN)		Buckling load (kN)	Failure load (kN)
		Eigenvalue	Riks	Hashin	LaRC05		
QI [(±45) ₂ /(90/0) ₂]s		2.28	2.24	15.56	12.61	2.19 ± 0.17	12.45 ± 0.82
Hybrid VSP [(±SFP) ₂ /(90/0) ₂]s	Method 1	2.50	2.48	18.26	14.64	2.39 ± 0.15(+9.1%)	14.54 ± 0.35(+16.8%)
		(+9.6%)	(+10.7%)	(+17.4%)	(+16.1%)		
	Method 2	2.47	2.44	17.43	13.90		
		(+8.3%)	(+8.9%)	(+11.8%)	(+10.2%)		

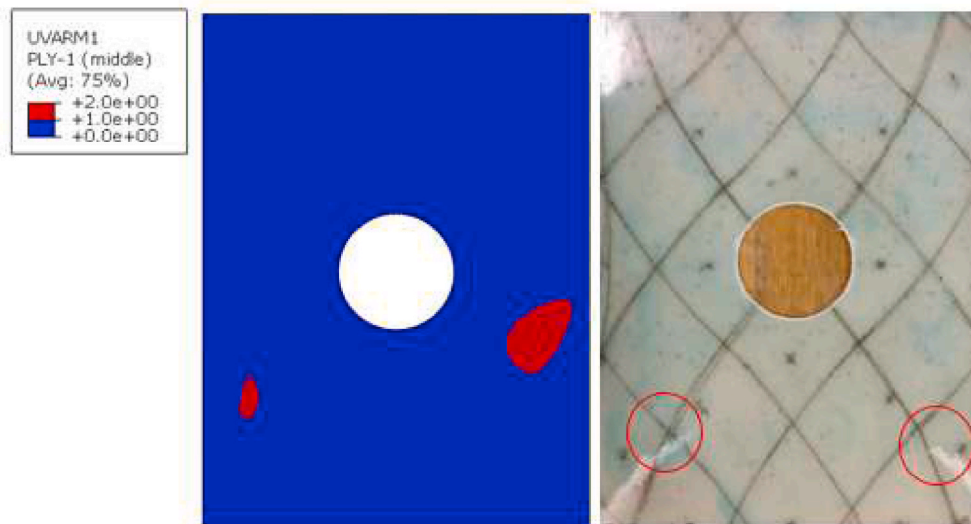


Fig. 14. Comparison between damage initiation locations predicted by LaRC05 and actual damages on the tested specimen (The specimen size is 300 mm × 400 mm).

prediction compared to the experimentally measured values. Because the increase in fibre volume fraction change is not included using Method 2 for the thickness versus shear angle behaviour, the predicted improvements of the hybrid laminates in buckling and failure loads are approximately 8% and 11% respectively.

The force-displacement curves in Fig. 13 indicate that the predicted stiffness is higher than the measured stiffness. Furthermore, damage initiation locations predicted by the LaRC05 model are slightly different from the position of cracks observed on the tested specimen, as shown in Fig. 14. There are several potential reasons that might explain these differences:

- In simulations, the material properties of each ply are based on unidirectional fibres, whereas the tested laminates are manufactured using woven fabric. Hence, the use of Classical Laminate Theory for a woven (crimped) fabric leads to an over-estimate of the stiffness [43], and consequently to a higher prediction of the buckling load [44]. Additionally, fibre waviness and fibre tow contact points in woven fabric composites are known to cause lower failure loads when compared to equivalent UD cross-ply laminates [43,45].
- Imperfections in the manufacturing process: For example the presence of voids in the moulded specimens can reduce failure load [46].
- Imperfections in the test conditions. For example, differences in the tightness of the bolts on the frames and clamps of the testing rig tended to create some distortion of the specimen, reducing the buckling load and causing slight differences in the buckled shapes (2nd mode) from one experiment to the next.

4. Conclusions

A novel manufacturing process, two-dimensional fabric steering, has been developed to manufacture variable stiffness panels. With the capability to simultaneously manipulate multiple layers of entire sheets of fabric, this technology offers a move towards high-volume production when compared to the tow-by-tow deposition currently employed by AFP technology, though technical innovation is required to reduce labour input using the proposed method. Manufacturing costs are also relatively low due to much lower capital costs compared to AFP. The

process is shown to be repeatable and guidelines on how to mitigate wrinkles during the forming process have been outlined. Using a multi-point manipulation method, good control is possible, as evidenced by the close visual match between the steered patterns generated by the SteerFab code and those manufactured in the lab. According to the buckling tests, the buckling and failure loads of the manufactured steered/straight hybrid laminates ($[(\pm SFP)_2/(90/0)_2]_s$) are improved by 9.1% and 16.8% respectively, compared to conventional QI laminates ($[(\pm 45)_2/(90/0)_2]_s$), though the hybrid laminates are ~4.6% heavier than the QI laminates. Similar level of improvements is predicted by the numerical analyses. Although the FE simulations using SteerFab/Abaqus do not closely predict experimental data due to several simplifications used in the modelling process (see Section 3.2), the numerical results reveal a similar trend with regard to the improvements offered by the two-dimensional steering process. Therefore, SteerFab is shown to be a useful numerical tool in optimising steered fibre patterns. In future SteerFab will be used to explore the effect of more complex steered fibre patterns on a variety of different structures.

CRediT authorship contribution statement

Zhaofei Xiao: Conceptualization, Methodology, Software, Validation, Formal analysis, Investigation, Data curation, Writing – original draft, Visualization. **Philip Harrison:** Conceptualization, Software, Resources, Writing – review & editing.

Declaration of competing interest

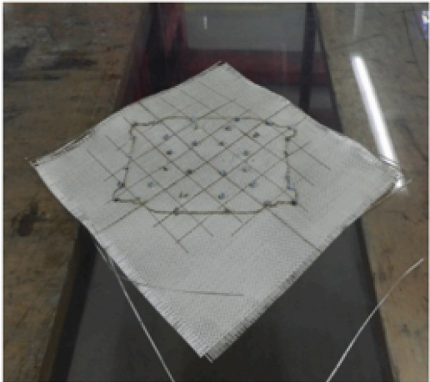
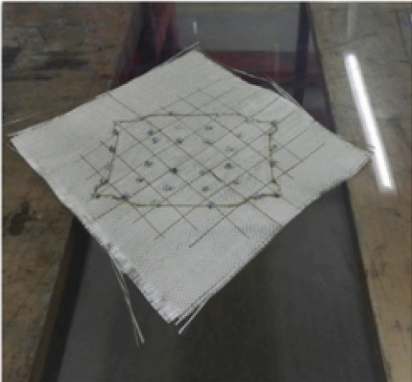
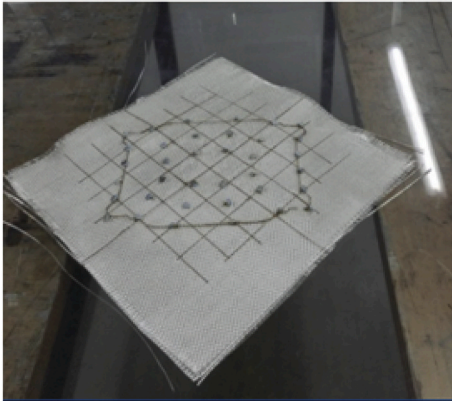
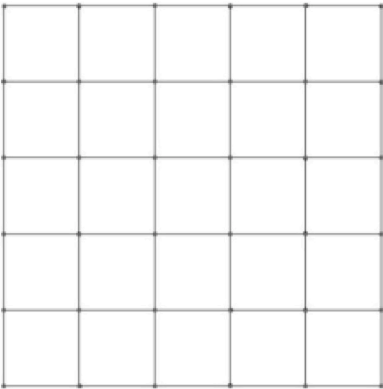
The authors declare that they have no known competing financial interests or personal relationships that could have appeared to influence the work reported in this paper.

Acknowledgements

The funding (EP/P021573/1) of this 2-D Forming of Low Cost Steered Fibre Laminates project from the Engineering and Physical Sciences Research Council (EPSRC) is gratefully acknowledge.

Appendix

A. Pictures of fabrics in the process repeatability test: Order 1 in Table 1 was used. The nodes manipulated at each step are highlighted in red and their displacement vectors are indicated by red arrows.

Initial state	
<div>Sample 1</div> 	<div>Sample 2</div> 
<div>Sample 3</div> 	<div>Nodes moved at this step</div> 
1st Step	(continued on next page)

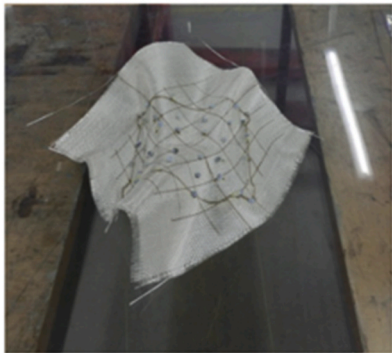
(continued)

Initial state

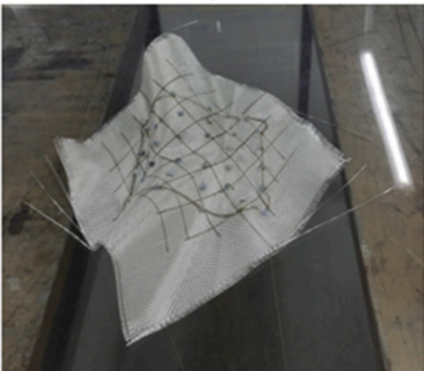
Sample 1



Sample 2

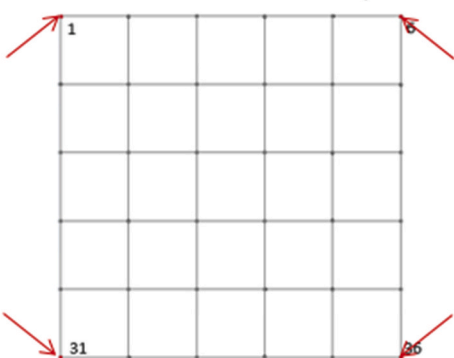


Sample 3



2nd Step

Nodes moved at this step



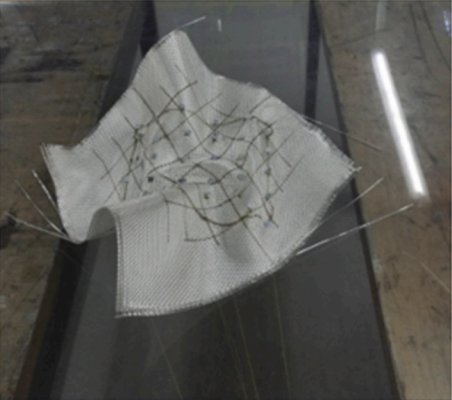
Sample 1



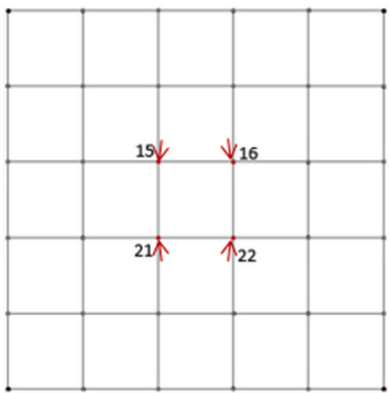
Sample 2



Sample 3



Nodes moved at this step



(continued on next page)

(continued)

Initial state

3rd Step

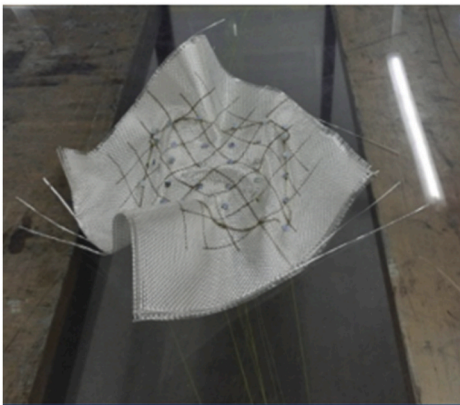
Sample 1



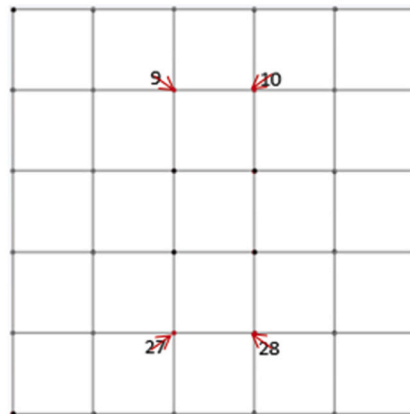
Sample 2



Sample 3



Nodes moved at this step



4th Step

(continued on next page)

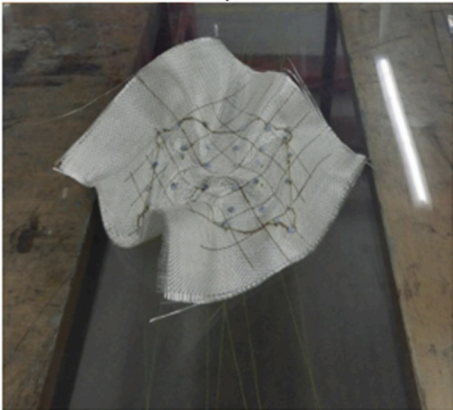
(continued)

Initial state

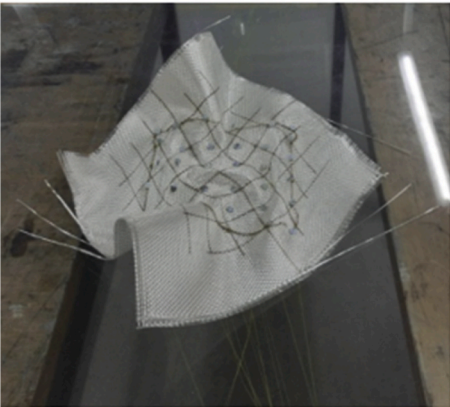
Sample 1



Sample 2

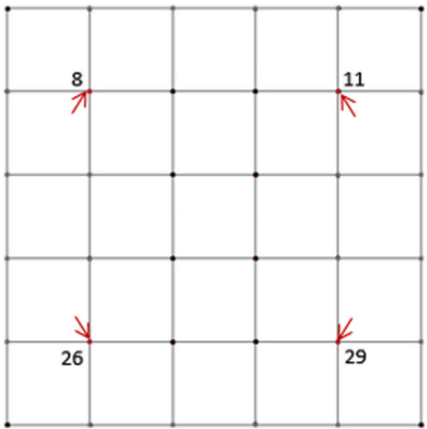


Sample 3



5th Step

Nodes moved at this step



(continued on next page)

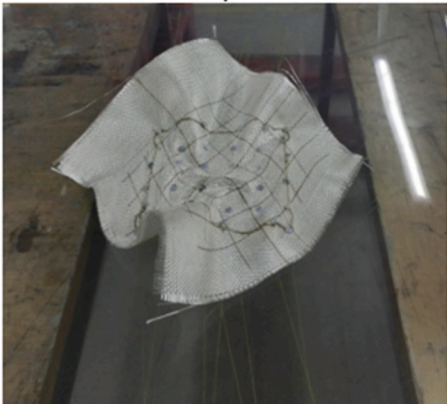
(continued)

Initial state

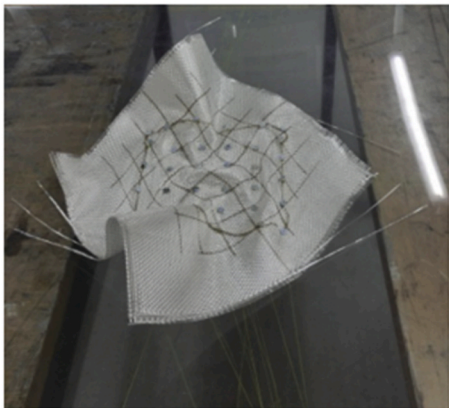
Sample 1



Sample 2



Sample 3



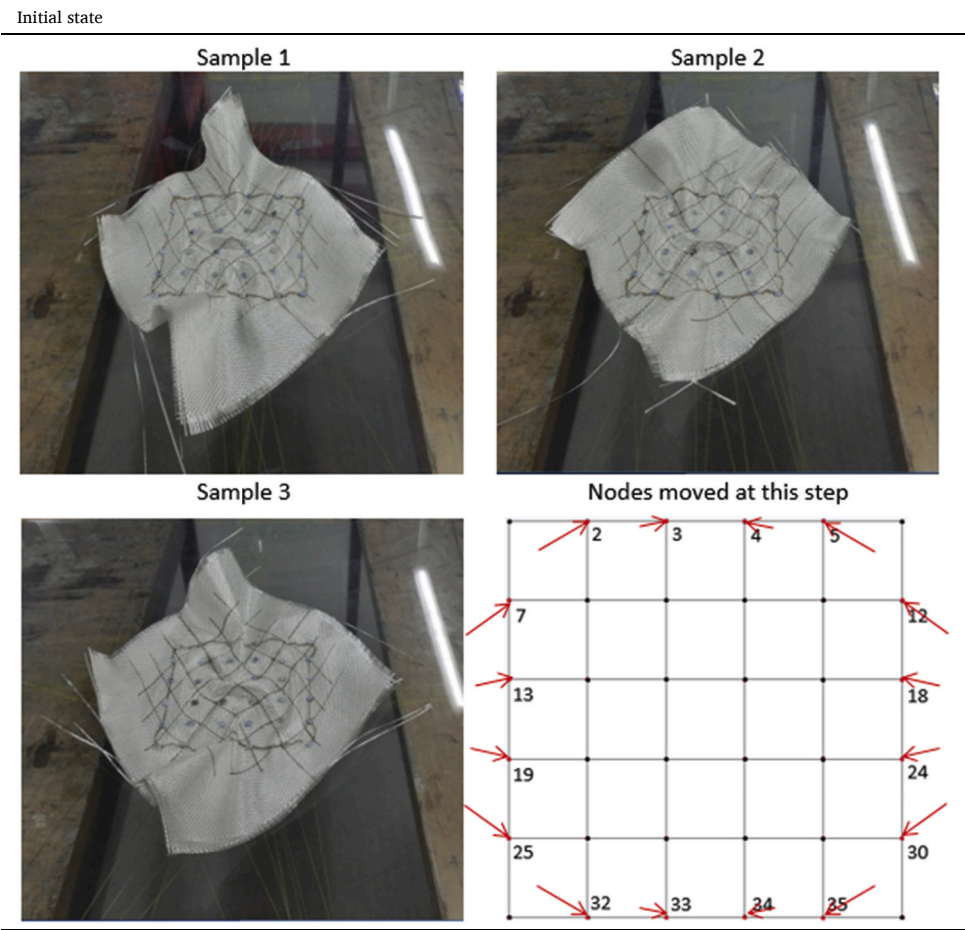
Nodes moved at this step



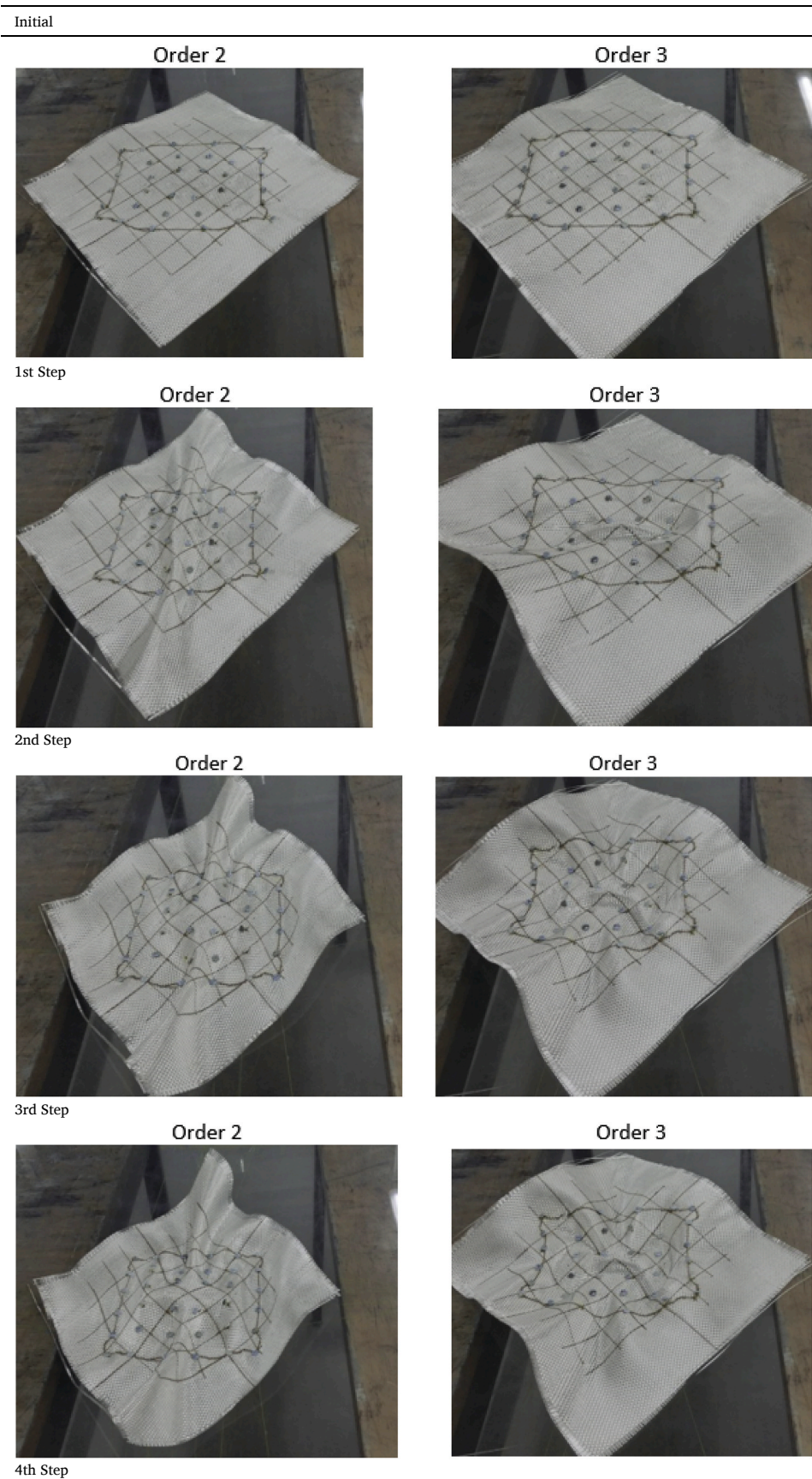
6th Step

(continued on next page)

(continued)



B. Pictures of fabric in the investigation of the effect of manipulation orders.

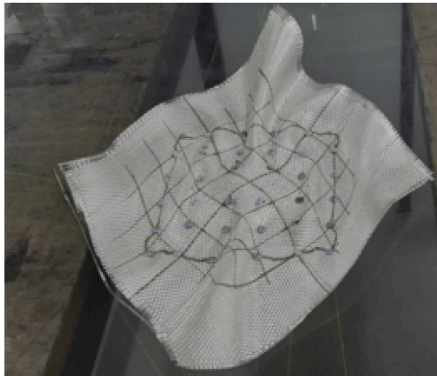


(continued on next page)

(continued)

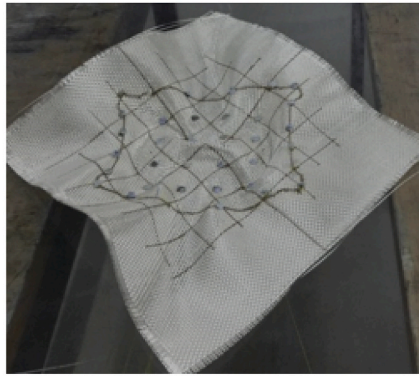
Initial

Order 2

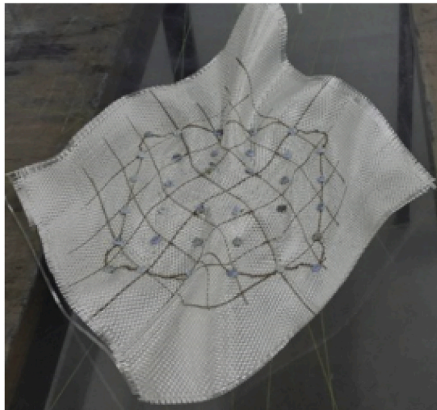


5th Step

Order 3

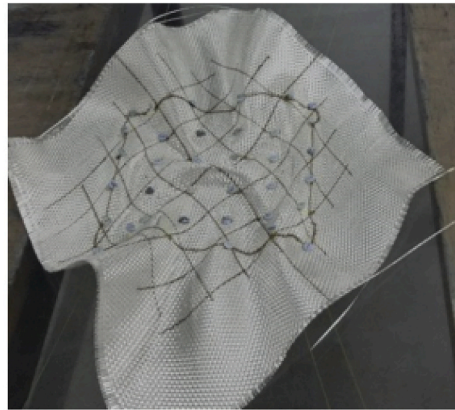


Order 2

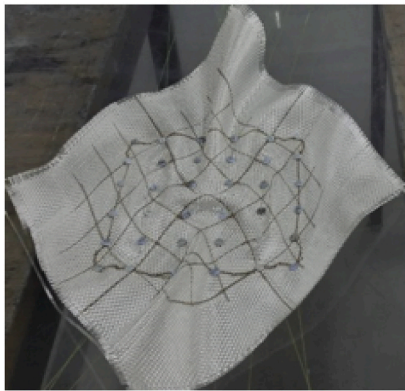


6th Step

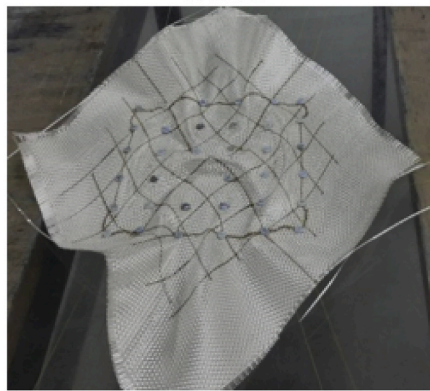
Order 3



Order 2



Order 3



References

- [1] Lopes CS, Gurdal Z, Camanho PP. Variable-stiffness composite panels: buckling and first-ply failure improvements over straight-fibre laminates. *Comput Struct* 2008; 86:897–907.
- [2] Xiao Z, Harrison P. Buckling analysis of variable stiffness panels manufactured by fabric steering technology. In: 22nd International Conference on Composites Materials (ICCM22); 2019. Melbourne, Australia.
- [3] Xiao Z, Harrison P. Design of buckling and damage resistant steered fibre composite laminates using trellis shear kinematics. *Compos Struct* 2021;260: 113526.
- [4] Lukaszewicz DHJA, Ward C, Potter KD. The engineering aspects of automated prepreg layup: history, present and future. *Compos B Eng* 2012;43(3):997–1009.
- [5] Tatting BF, Gurdal Z. Design and manufacture of elastically tailored tow placed plates. Tech. Rep., NASA 2002. NASA/CR-2002-211919.
- [6] Gurdal Z, Tatting BF, Wu CK. Variable stiffness composite panels: Effects of stiffness variation on the in-plane and buckling response. *Compos Appl Sci Manuf* 2008;39(5):911–22.
- [7] Wu K, Tatting B, Smith B, Stevens R, Occhipinti G, Swift J, Achary D, Thornburgh R. Design and Manufacturing of tow-steered composite shells using fiber placement. In: 50th AIAA/ASME/ASCE/AHS/ASC structures, structural dynamics, and materials conference; 2009 [American Institute of Aeronautics and Astronautics].
- [8] Lopes CS, Camanho PP, Gurdal Z, Tatting BF. Progressive failure analysis of tow-placed, variable-stiffness composite panels. *Int J Solid Struct* 2007;44:8493–561.
- [9] Weaver PM, Potter KD, Hazra K, Savarymuthapulle MAR, Hawthorne MT. Buckling of variable angle tow plates: from Concept to experiment. In: 50th AIAA structures, structural dynamics, and materials conference; 2009 [California].
- [10] Alhajahmad A, Abdalla MM, Gurdal Z. Optimal Design of tow-placed fuselage Panels for maximum Strength with buckling considerations. *J Aircraft* 2010;47(3): 775–82.

- [11] Coburn BH, Wu Z, Weaver PM. Buckling analysis of stiffened variable angle tow panels. *Compos Struct* 2014;111:259–70.
- [12] Stanford BK, Jutte CV. Aeroelastic tailoring via tow steered composites. Hampton, VA: NASA Langley Research Center; 2014.
- [13] Kim B, Hazra K, Weaver P, Potter K. Limitations of fibre placement techniques for variable angle tow composites and their process-induced defects. In: 18th ICCM; 2011 [Jeju, KR].
- [14] Kim BC, Potter K, Weaver PM. Continuous tow shearing for manufacturing variable angle tow composites. *Compos Appl Sci Manuf* 2012;43(8):1347–56.
- [15] Kim BC, Weaver PM, Potter K. Manufacturing characteristics of the continuous tow shearing method for manufacturing of variable angle tow composites. *Compos Appl Sci Manuf* 2014;61:141–51.
- [16] Stodieck O, Francois G, Heathcote D, Zypeloudis E, Kim BC, Rhead A, Cleaver D, Cooper J. Experimental Validation of tow-steered composite Wings for aeroelastic design. In: International Forum on Aeroelasticity and structural dynamics, IFASD; 2017.
- [17] Boisse P. *Advances in composites Manufacturing and process design*. Woodhead Publishing; 2015.
- [18] Van Der Weeën F. Algorithms for draping fabrics on doubly-curved surfaces. *Int J Numer Methods Eng* 1991;31(7):1415–26.
- [19] Boisse P, Gasser A, Hivet G. Analyses of fabric tensile behaviour: determination of the biaxial tension-strain surfaces and their use in forming simulations. *Compos Appl Sci Manuf* 2001;32(10):1395–414.
- [20] Cao J, Akkerman R, Boisse P, Chen J, Cheng HS, de Graaf EF, Gorczyca JL, Harrison P, Hivet G, Launay J, Lee W, Liu L, Lomov SV, Long A, de Luycker E, Morestin F, Padvoiskis J, Peng XQ, Sherwood J, Stoilova T, Tao XM, Verpoest I, Willems A, Wiggers J, Yu TX, Zhu B. Characterization of mechanical behavior of woven fabrics: Experimental methods and benchmark results. *Compos Appl Sci Manuf* 2008;39(6):1037–53.
- [21] Harrison P, Abdiwi F, Guo Z, Potluri P, Yu WR. Characterising the shear-tension coupling and wrinkling behaviour of woven engineering fabrics. *Compos Appl Sci Manuf* 2012;43(6):903–14.
- [22] Harrison P, Wiggers J, Long AC. Normalization of shear test Data for rate-independent compressible fabrics. *J Compos Mater* 2008;42(22):2315–44.
- [23] d'Agostino. M.V., I. Giorgio, L. Greco, A. Madeo, and P. Boisse, Continuum and discrete models for structures including (quasi-) inextensible elasticae with a view to the design and modeling of composite reinforcements. *Int J Solid Struct* 2015; 59:1–17.
- [24] Harrison P. Modelling the forming mechanics of engineering fabrics using a mutually constrained pantographic beam and membrane mesh. *Compos Appl Sci Manuf* 2016;81:145–57.
- [25] Lomov SV, Verpoest I. Model of shear of woven fabric and parametric description of shear resistance of glass woven reinforcements. *Compos Sci Technol* 2006;66(7): 919–33.
- [26] Sachs U, Akkerman R, Fetfatsidis K, Vidal-Sallé E, Schumacher J, Ziegmann G, Allaoui S, Hivet G, Maron B, Vanclooster K, Lomov SV. Characterization of the dynamic friction of woven fabrics: Experimental methods and benchmark results. *Compos Appl Sci Manuf* 2014;67:289–98.
- [27] Chen Z-R, Ye L. A micromechanical compaction model for woven fabric preforms. Part II: Multilayer. *Compos. Sci. Technol.* 2006;66(16):3263–72.
- [28] Harrison P, Gonzalez Camacho LF. Deep draw induced wrinkling of engineering fabrics. *Int J Solid Struct* 2021;212:220–36.
- [29] Cooper DNE. A bias extension test. *Textil Res J* 1963;33(4):315–7.
- [30] Lebrun G, Bureau MN, Denault J. Evaluation of bias-extension and picture-frame test methods for the measurement of intraply shear properties of PP/glass commingled fabrics. *Compos Struct* 2003;61(4):341–52.
- [31] Boisse P, Hamila N, Guzman-Maldonado E, Madeo A, Hivet G, dell'Isola F. The bias-extension test for the analysis of in-plane shear properties of textile composite reinforcements and prepregs: a review. *Int J Material Form* 2017;10(4):473–92.
- [32] Boisse P, Hamila N, Vidal-Sallé E, Dumont F. Simulation of wrinkling during textile composite reinforcement forming. Influence of tensile, in-plane shear and bending stiffnesses. *Compos. Sci. Technol.* 2011;71(5):683–92.
- [33] Harrison P, Taylor E, Alsayednoor J. Improving the accuracy of the uniaxial bias extension test on engineering fabrics using a simple wrinkle mitigation technique. *Compos Appl Sci Manuf* 2018;108:53–61.
- [34] Kim BC, Weaver PM, Potter K. Computer aided modelling of variable angle tow composites manufactured by continuous tow shearing. *Compos Struct* 2015;129: 256–67.
- [35] Rasband WS. ImageJ. 1997-2018 [cited 2020]. Available from, <https://imagej.nih.gov/ij/>.
- [36] Riks E. An incremental approach to the solution of snapping and buckling problems. *Int J Solid Struct* 1979;15(7):529–51.
- [37] Pickett AK. *Process and mechanical modelling of engineering composites*. IFB, University Stuttgart; 2017.
- [38] Hashin Z. Failure criteria for unidirectional fibre composites. *J Appl Mech* 1980;47: 329–34.
- [39] Pinho ST, Darvizeh R, Robinson P, Schuecker C, Camanho PP. Material and structural response of polymer-matrix fibre-reinforced composites. *J Compos Mater* 2012;46:2313–41.
- [40] Pinho S, Vyas G, Robinson P. Material and structural response of polymer-matrix fibre-reinforced composites: Part B. *J Compos Mater* 2013;47(6–7):679–96.
- [41] Daniel IM, Ishai O. *Engineering mechanics of composite materials*. second ed. Oxford university press; 2006.
- [42] Bulson PS. *The stability of flat plates*. London: Chatto & Windus.; 1970.
- [43] Wijskamp S. Shape distortions in composites forming. In: *Mechanical engineering, division of design, production and manufacturing*. The Netherlands: University of Twente; 2005.
- [44] Leissa AW. An Overview of composite plate buckling. In: Marshall IH, editor. *Composite structures 4: volume 1 analysis and design studies*. Dordrecht: Springer Netherlands; 1987. p. 1–29.
- [45] Adumitroaie A, Barbero EJ. Stiffness and strength prediction for plain weave textile reinforced composites. *Mech Adv Mater Struct* 2012;19:169–83.
- [46] de Almeida SFM, Neto ZD. Effect of void content on the strength of composite laminates. *Compos Struct* 1994;28(2):139–48.